

Decoding the minimum-yield position of high-order harmonic generation from H_2^+ with a large internuclear distance

Ting-Ting Fu, Yue Qiao , Jun Wang , Fu-Ming Guo, and Yujun Yang *

Institute of Atomic and Molecular Physics, Jilin University, Changchun 130012, China

and Jilin Provincial Key Laboratory of Applied Atomic and Molecular Spectroscopy (Jilin University), Changchun 130012, China

 (Received 29 March 2023; revised 21 July 2023; accepted 13 September 2023; published 26 September 2023)

By numerically solving the time-dependent Schrödinger equation, we investigate the harmonic emission of H_2^+ with a large internuclear distance in the midinfrared laser field. We find that multiple minima are observed in the high-order harmonic spectra. As the laser wavelength and intensity increase, the harmonic minima gradually shift to the high-energy region, which is different from the position of the minima predicted by the originally studied two-center interference. We modify the formula so that the position of the minimum yield of high-order harmonics generated at large internuclear distances can be accurately interpreted by our modified formula. Consequently, by using the harmonic minimum, it is feasible to determine the parameters of the driving laser and the bond length of the molecule. Additionally, we discuss the impact of nuclear motion and laser pulse duration on the position of harmonic minimum.

DOI: [10.1103/PhysRevA.108.033115](https://doi.org/10.1103/PhysRevA.108.033115)

I. INTRODUCTION

A high-order harmonic will be generated when atoms, molecules, and solid materials are irradiated by a strong laser pulse [1–7]. As the harmonic energy increases, the intensity of the harmonic spectrum shows a plateau structure. Therefore, high-order harmonics are desktop coherent light sources whose wavelengths range from extreme ultraviolet to soft x rays [8–11]. Due to a plateau that appears in a wide frequency range with roughly the same intensity, high-order harmonics are used to generate ultrashort attosecond laser pulses [12–14], which could be one of the most powerful tools to detect ultrafast electronic dynamics [15–20].

The semiclassical three-step model [21] provides a clear explanation for how high-order harmonic generation works: Through tunnel ionization, the intense laser field rips a valence electron off an atom or molecule. The ionized electron is accelerated in the laser field, which soon reverses its sign and returns to the parent ion, then emits a harmonic photon. From the perspective of the emission mechanism, one can find that the instantaneous structural characteristics of the atoms and molecules are encoded in the harmonic spectra. The recolliding electron acts as a probe pulse, and the photons that are released serve as the signal that communicates information about the molecule. Therefore, the electronic orbitals of the molecule are imaged by a tomography scheme using high-order harmonics [17,22].

One important application of harmonics in molecular structure parameter detection is probing the internuclear distance using the harmonic minimum. The local minimum features in harmonic spectra have been widely investigated [23–29]. Higuete *et al.* [25] investigated the Cooper-like minimum of the

harmonic spectra from an argon atom irradiated by a strong laser field. They found that the harmonic minimum is unaffected by the laser parameters. For the molecular harmonic, Smirnova *et al.* [26] found the harmonic minimum is generated from the interference of multiple electronic orbitals. The generation of this minimum is not sensitive to the alignment of the molecules. The parameters of the driving laser pulse play an important role in the position of the harmonic minimum.

Another kind of harmonic minimum is generated from the interference of the two centers in a diatomic molecule [30–35]. When the ionized wave packet returns to the molecular ion, two harmonic sources are generated due to the rescattering with different nuclei. The accumulated phase difference between the two central harmonics is $pR \cos \theta$. Here, $p = 2\pi \hbar/\lambda$ [35] is the amplitude of the electron momentum, R is the distance between two nuclei, and θ is the angle between the molecular axis and the laser polarization direction. \hbar is the reduced Planck constant, and λ is the de Broglie wavelength. The minima appear in the harmonic spectrum when the equation is satisfied. There is a clear correspondence between the position of the harmonic minimum and the bond length of the molecules. Since the energy of the harmonic minimum is not sensitive to the laser parameters, it is possible to probe the molecular bond length with the harmonic minimum.

Since this phenomenon was first observed by Lein *et al.* [34–36], it has been studied theoretically and experimentally. Recently, it was found that the cutoff energy of the harmonic emission plateau can be greatly expanded for long-range molecular ions. Therefore, research on high-order harmonic generation from long-range molecular ions is increasing. Cui *et al.* investigated high-order harmonic generation of H_2^+ and HeH^{2+} [37] (see also the work by Han and Madsen [38]). They found that excited states play an important role in high-order harmonic generation, especially in the case of large bond lengths. Theoretical investigations of H_2^+ at large

*yangyj@jlu.edu.cn

internuclear distances provide a comprehensive approach to explore the strong-field ionization and high-order harmonic generation mechanisms in atoms and molecules [39–46]. Bandrauk and colleagues [39,40] discussed the impact of internuclear distance on strong-field ionization in H_2^+ . It is worth noting that recently, Silva *et al.* [44] discussed the influence of the laser electric field on the dissociation of diatomic molecules. They showed that light induced the generation of permanent dipoles to produce even harmonics. Our research focuses on the influence of the laser field on the minimum position of the H_2^+ harmonic spectrum with a large internuclear distance. In this work, the harmonic minima of long-range molecular ions are systematically investigated. As the laser's wavelength and intensity increase, the harmonic minimum progressively moves toward the high-energy region. With the different local area analyses and the time-frequency analysis of the harmonic, we explain the reasons for the variation of these minima with the laser parameters. Our updated two-center interference formula accurately predicts the position of minimum at a large internuclear distance. This paper is organized as follows: Sec. II discusses the numerical methods used in this paper, Sec. III presents the harmonic emission spectra and the mechanism analysis of the minimum shift, and the last section summarizes the paper's content. (Unless otherwise stated, atomic units are used throughout this paper.)

II. SCHEME AND THEORETICAL METHOD

In the electric dipole approximation and the velocity gauge, the time-dependent Schrödinger equation for H_2^+ is [47,48]

$$i \frac{\partial}{\partial t} \psi(x, t) = H(x, t) \psi(x, t). \quad (1)$$

In the case of fixed nuclei, the Hamiltonian operator of the system is

$$\begin{aligned} H(x, t) &= \frac{\mathbf{p}^2}{2} + V(x) + \mathbf{p}\mathbf{A}(t) \\ &= \frac{\mathbf{p}^2}{2} + \frac{-1}{\sqrt{(x - R/2)^2 + a}} \\ &\quad + \frac{-1}{\sqrt{(x + R/2)^2 + a}} + \mathbf{p}\mathbf{A}(t). \end{aligned} \quad (2)$$

In the case of nuclear motion, the Hamiltonian operator of the system is [49]

$$\begin{aligned} H'(x, t) &= \frac{\mathbf{p}^2}{2} + V'(x) + \mathbf{p}\mathbf{A}(t) \\ &= \frac{\mathbf{p}^2}{2} + \frac{-1}{\sqrt{(x + R_1(t))^2 + a'}} \\ &\quad + \frac{-1}{\sqrt{(x + R_2(t))^2 + a'}} + \mathbf{p}\mathbf{A}(t). \end{aligned} \quad (3)$$

It should be pointed out that the solution given by Eq. (3) is an approximation considering the motion of the nuclei. Corso *et al.* verified the effectiveness of harmonic calculations by comparing the method using the three-dimensional Schrödinger equation with this scheme [49]. For higher intensity and longer pulses, harmonic emission becomes more

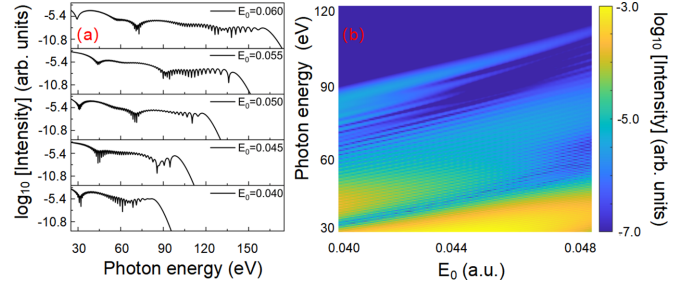


FIG. 1. (a) The effect of different laser-field amplitudes on harmonic energy and intensity for a given laser frequency. (b) Variation of harmonic intensity with driving laser amplitude from 0.04 to 0.048.

complex [50,51] due to factors such as increased ionization and the complexity of nuclear dynamics. Therefore, further improvement of this scheme [49] is needed. However, the driving laser pulse used in our study is short, and the intensity is not high, so we adopt Eq. (3) to study the change in the minimum position in the case of nuclear motion.

Here, $R(t) = R + \Delta R \sin(\omega_N t)$, $R_1(t) = -R_2(t) = R(t)/2$, the soft-core parameter $a = 2.1$, $a' = 2$, ω_N is the oscillation frequency, and internuclear distance $R = 9$, and the nuclei displacement from the nuclear position is $\Delta R = 0.15$ [49]. The corresponding ground-state energy of the system is -16.66 eV [52].

The vector potential is $A(t) = -\int E(t)dt$, where $E(t)$ is the linearly polarized laser electric field: $E(t) = eE_0 f(t) \sin(\omega_0 t)$. Here, E_0 and ω_0 are the peak amplitude and angular frequency of the laser electric field, and e is a unit vector along the x axis. The envelope of the laser pulse is $f(t) = \sin^2(\omega_0 t/2N)$, where N is the period number of the laser pulse.

The time-dependent wave function is obtained with the numerical solution by using the split-operator scheme [48]. By using the time-dependent wave function, the dipole in acceleration form can be calculated as

$$\begin{aligned} a(t) &= \frac{d^2}{dt^2} \langle \psi(x, t) | x | \psi(x, t) \rangle \\ &= \langle \psi(x, t) | -\frac{dV(x)}{dx} - E(t) | \psi(x, t) \rangle. \end{aligned} \quad (4)$$

The harmonic spectra are obtained with Fourier transform of the time-dependent dipole:

$$P(\omega) \propto \left| \frac{1}{\omega^2(t_f - t_i)} \int_{t_i}^{t_f} a(t) \exp(-i\omega t) dt \right|^2 \quad (5)$$

III. RESULTS AND DISCUSSION

The harmonic spectra generated by H_2^+ are presented in Fig. 1(a). The frequency of the driving laser is 0.019, $N = 2$, and the peak amplitudes of the laser fields are 0.04, 0.045, 0.05, 0.055, and 0.06. For harmonic spectra generated from a driving laser with different intensities, one can clearly observe the minima. It is worth noting that, as the driving laser amplitude increases, the harmonic minima shift continuously. In order to observe the significance of variations in harmonic minima, we calculated the harmonic spectra by changing the

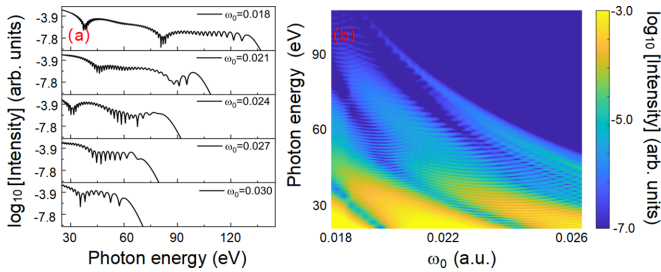


FIG. 2. (a) The harmonic intensity versus harmonic energy for various laser frequencies at a given laser intensity for $N = 2$. (b) Variation of harmonic intensity with laser frequency from 0.018 to 0.026 for $N = 2$.

electric-field peak amplitude from $E_0 = 0.04$ to 0.048 with a step size of 0.0002, as shown in Fig. 1(b). We discovered that the harmonic minimum gradually advances towards the high-energy area as the laser intensity rises.

Furthermore, we investigate the role of the driving laser frequency in the harmonic minimum. Figure 2(a) presents the harmonic emission spectra with the same laser intensity and different frequencies. The peak amplitude of the laser pulse is 0.05. The frequencies of the laser field are 0.018, 0.021, 0.024, 0.027, and 0.030. For a laser with different frequencies, the minima are also found in the harmonic spectra. Moreover, the position of the harmonic minimum is vastly different. As the driving laser frequency increases, the number of harmonic minima decreases. We further systematically investigate the variation of the harmonic intensity with the driving laser frequency in the range of 0.018 to 0.026. Our research demonstrates that as laser frequency increases, the harmonic minimum steadily moves into the low-energy region.

According to the aforementioned research, as laser intensity increases or driving laser frequency decreases, the harmonic minimum position moves into the high-energy zone. This behavior is similar to the ponderomotive energy of electrons for given driving laser parameters: $U_p = E_0^2 / (4\omega_0^2)$. Consequently, the behavior of the harmonic emission spectrum with the same U_p as the laser pulse is investigated. The corresponding results are presented in Fig. 3. The laser frequencies are 0.019, 0.021, 0.023, 0.025, and 0.028. Since equal U_p is selected, the cutoff frequency of the plateau appears at the same position. More importantly, the position of the minimum of the harmonic spectrum is the same. The positions of the harmonic minima are around 31 and 68 eV. We examined these minima from a time-domain perspective to observe the minima's properties more thoroughly. The peak amplitude of the laser electric field is 0.045, $N = 2$, and the frequency of the driving laser is 0.019. The harmonic spectrum of H_2^+ irradiated by a laser pulse is presented in Fig. 4(a). Two minima exist in the harmonic emission spectrum, and their energies are 47 and 87 eV. Moreover, the photon energy distribution of the minimum in the high-energy region (87 eV) is much wider. Furthermore, using time-frequency analysis [Fig. 4(b)], three minima are observed. The energies of the minima are 47, 87, and 86.6 eV. In particular, in the high-energy region, there is a minimum for each of the long and short trajectories, which causes this minimum to be wider. This harmonic feature is significantly different from

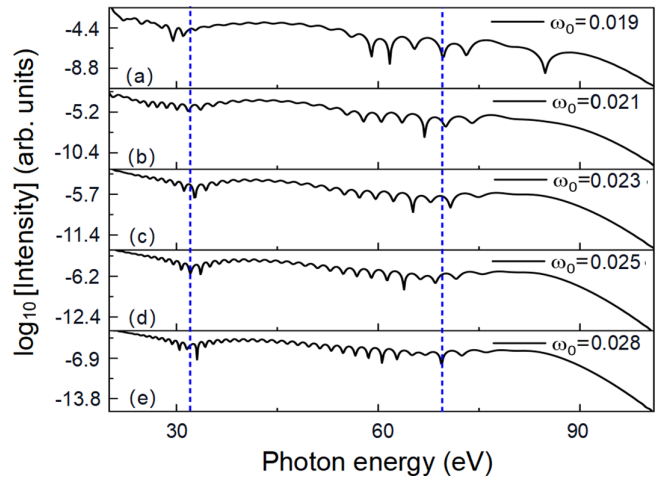


FIG. 3. Harmonic spectra of H_2^+ when $U_p = 1.12$ a.u. and $N = 2$, with an internuclear distance of 9. The laser frequency and field intensity are adjusted so that the value of U_p is the same. The horizontal axis is the photon energy, and the vertical axis is the harmonic intensity. (a)–(e) represent laser frequencies of 0.019, 0.021, 0.023, 0.025, and 0.028 respectively. The blue dashed line represents the position of the minima.

the commonly observed minimum (red dashed line), which is calculated with the original two-center interference equation.

For the sake of gaining insight into the mechanism of the variation of harmonic minima with laser pulse parameters, we analyze the amplitude as well as phase of the two centers of the interference. The wave functions of the ground state $\psi_1(x)$ and the first excited state $\psi_2(x)$ are presented in Fig. 5(a). According to the multichannel dynamic model, we can obtain the localized states' wave functions of the two centers by linearly combining the ground state and the first excited state [37,38]: $\psi_R(x) = (1/\sqrt{2})[\psi_1(x) - \psi_2(x)]$, $\psi_L(x) = (1/\sqrt{2})[\psi_1(x) + \psi_2(x)]$. Simultaneously, the total

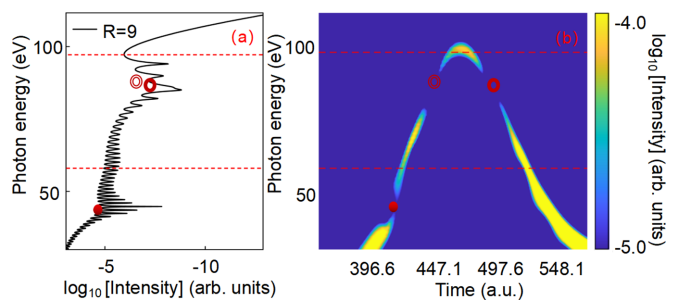


FIG. 4. Harmonic spectrum and time-frequency analysis of a driving laser with $E_0 = 0.045$, $\omega_0 = 0.019$, and $N = 2$ when the driving laser illuminates H_2^+ with an internuclear distance of 9. (a) The harmonic spectrum between 30 and 115 eV is shown; the horizontal axis is the harmonic intensity, and the vertical axis is the photon energy. (b) The corresponding time-frequency analysis of (a). The red dashed line represents the position of the minima obtained from the original two-center interference model [35]. The red solid circle, double circle, and semisolid circle correspond to the positions of the minima obtained with our modified two-center interference formula.

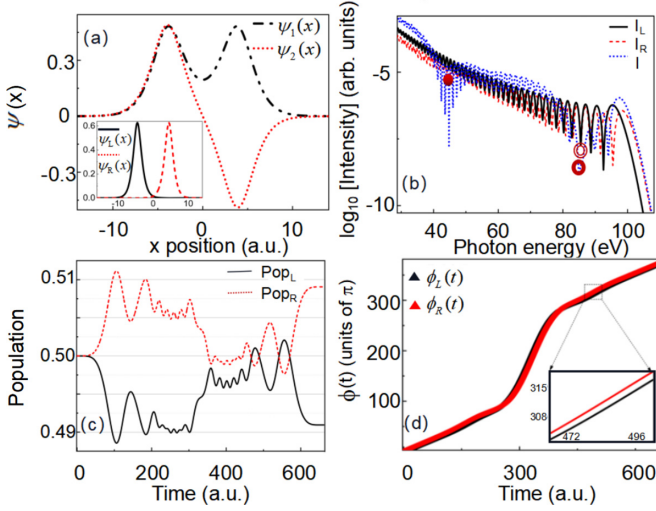


FIG. 5. Results for dividing H_2^+ into two localized states at a laser-field amplitude of 0.045, a frequency of 0.019, and $N = 2$. (a) The wave functions of the ground state (black dot-dashed line) as well as the first excited state (red dotted line). The inset shows the localized state on the left $\psi_L(x)$ and the localized state on the right $\psi_R(x)$. (b) The harmonic spectra of the right-hand part (I_R), the left-hand part (I_L), and the two localized states together (I). The red solid circle, double circle, and semisolid circle represent the positions of the minima. (c) The time-dependent population of $\psi_L(x)$ (black solid line) and $\psi_R(x)$ (red dotted line). (d) The phase of the left nuclei ϕ_L (black triangles) and the phase of the right nuclei ϕ_R (red triangles).

wave function can be expressed as

$$\psi(x, t) = C_L \psi_L(x) + C_R \psi_R(x) + \psi_{\text{res}}(x, t), \quad (6)$$

where $C_R(t) = \langle \psi_R(x) | \psi(x, t) \rangle$, $C_L(t) = \langle \psi_L(x) | \psi(x, t) \rangle$, and $\psi_{\text{res}}(x, t)$ is the residual part of $\psi(x, t)$, whose value is small enough to be roughly disregarded.

According to Eq. (6), the local wave functions for the two centers of H_2^+ are presented in the inset of Fig. 5(a). With a large internuclear distance, the two centers of H_2^+ can be well separated by taking advantage of this scheme. By using the wave-function expansion scheme, one can obtain the harmonic emission spectra of two localized states. The corresponding spectra are presented in Fig. 5(b). Moreover, it can be seen that the harmonic spectra generated by the two localized states have nearly the same intensity, and no minimum is observed. However, the obvious minima at 47, 87, and 86.6 eV can be observed in the harmonics generated by the coherence of the two localized states. The interference of the high-order harmonics is related to the population and phase in each localized state. Therefore, we further calculate the time-dependent evolution of the population and phase of these two parts. The time-dependent populations of the two parts are presented in Fig. 5(c). In addition, we find that the populations of these two localized states oscillate around 0.5. Accordingly, the harmonic intensities generated by these two localized states are close. However, the phases of two localized states are unequal, as shown by Fig. 5(d).

To illustrate the physical mechanism of change in the position of the minimum, we further calculate the time-dependent

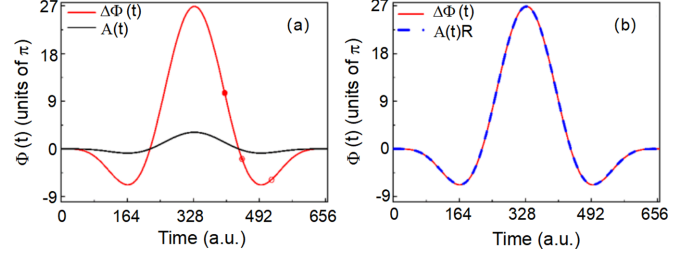


FIG. 6. The relationship between the phase difference between two local states and the vector potential when $E_0 = 0.045$, $\omega_0 = 0.019$, $N = 2$, and the internuclear distance $R = 9$. (a) The phase difference between the two parts and the vector potential of the laser pulse. The moments of the red solid circle, double circle, and semisolid circle correspond to the moments at the position of the minima in Fig. 4(b). (b) The phase difference between the two localized states and the result calculated using $A(t)R$, $R = 9$.

evolution, as shown by the red solid line in Fig. 6(a). It is seen that the phase difference oscillates with time. The phase difference reaches the maximum at an instant of 328 a.u. The effect of this phase difference causes the interference minima to shift. The conventional two-centered minima position is obtained with the equation $R \cos \theta / \lambda = (n - 1/2)$ ($n = 1, 2, 3, \dots$). In this model, the phase differences between the two localized states are not considered. In this condition, the obtained minimum's position is not consistent with numerical simulation. Therefore, we modify the formula for the harmonic minimum to $R/\lambda + \Delta\Phi(t)/2\pi = (n - 1/2)$ ($n = 1, 2, 3, \dots$). Inserting the phase differences of the respective three moments in Fig. 6(a) into the modified equation, the positions of the three minima in Fig. 5(b) can be obtained separately. Here, $R = 9$, and $I_p = -0.612$. Specifically, when time is 404 a.u., Fig. 6(a) indicates that the phase is $\Delta\Phi(t) = \phi_L - \phi_R = 11.28\pi$. Here, ϕ_L and ϕ_R can be written as $\phi_i = \text{atan}(\text{imag}(a_i), \text{real}(a_i))$ ($i = L, R$), where $a_i(t) = \frac{d^2}{dt^2} \langle \psi_i(x, t) | x | \psi_i(x, t) \rangle$ ($i = L, R$). Adding the phase difference to the modified formula, where $n = 4$, according to formulas $p = 2\pi \hbar / \lambda$ and $E = p^2/2 + I_p$, we can get the minimum position at 47 eV. Here, I_p is the ground-state energy. Similarly, when time is 447 a.u., according to the red double circle in Fig. 6(a) with phase difference $\Delta\Phi(t) = -1.517\pi$, which is carried into the modified equation, where $n = 3$, we can obtain the minimum position at 87 eV. When time is 525 a.u., according to the red semisolid circle in Fig. 6(a) with phase difference $\Delta\Phi(t) = -5.5\pi$ and $n = 1$ in the formula, we can obtain the minimum at 86.6 eV. As elaborated above, the position of the minimum calculated according to the modified equation can be well matched with the position of the harmonic spectrum minima.

The above analysis indicates that this phase difference $\Delta\Phi(t)$ is related to the laser parameters. For the field-free condition, the phase difference between the two localized states is zero. With the action of the driving laser, a new potential energy is induced, and this potential energy can be expressed for both localized states as $\int_{-\infty}^{t'} -E(t)Rdt$, where t' is the instant of emitting light. Since $A(t') = -\int_{-\infty}^{t'} E(t)dt$, this potential energy can be expressed as $\int_{-\infty}^{t'} E(t)Rdt = A(t')R$.

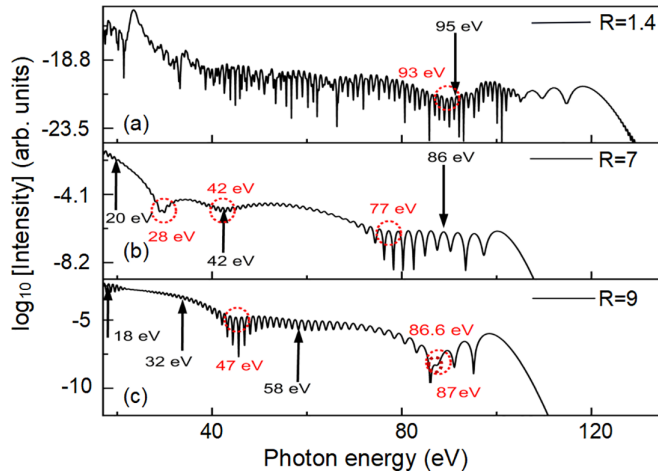


FIG. 7. The minimum energy variation at different internuclear distances when $E_0 = 0.045$, $\omega_0 = 0.019$, and $N = 2$. The red dashed circles represent the minima calculated using the modified formula. The black arrows calculate the minima of energy according to the original two-center interference formula. (a) $R = 1.4$ ($I_p = -1.28$), (b) $R = 7$ ($I_p = -0.64$), and (c) $R = 9$ ($I_p = -0.612$).

The laser electric field induces a potential-energy difference between the two localized states, resulting in a nonzero phase difference between these two parts, and this phase difference can be expressed as $\Delta\Phi(t) = A(t)R$. In Fig. 6(b), we give the phase difference $\Delta\Phi(t) = \phi_L - \phi_R$ and the numerical calculation $A(t)R$, from which we can confirm they are consistent. Thus, the energy of the harmonic minima for molecular ions with large internuclear distance is tightly related to the laser parameters and can be explained by applying our modified equation:

$$R/\lambda + [A(t)R]/2\pi = (n - 1/2) \quad (n = 1, 2, 3, \dots) \quad (7)$$

To verify the accuracy of the modified formula further, we calculate the harmonic emission spectra for $R = 1.4$, $R = 7$, and $R = 9$, where I_p with different internuclear distances give in Ref. [52]. The harmonic emission spectra with different internuclear distances are represented in Fig. 7. It can be observed that the cutoff energy changes because of the different I_p . More importantly, the position of the minima in the harmonic spectrum can be calculated using the modified two-center interference formula. At $R = 1.4$ [Fig. 7(a)], the minimum's position obtained from the original two-center interference is at 95 eV ($n = 1$), while the modified energy is at 93 eV ($n = 1$), which are nearly coincident results. When $R = 7$ [Fig. 7(b)], the original equation calculates the minima at 20 eV ($n = 1$), 42 eV ($n = 2$), and 86 eV ($n = 3$), while the modified equation calculates the minima at 28 eV ($n = 5$), 42 eV ($n = 4$), and 77 eV ($n = 3$), respectively. When $R = 9$ [Fig. 7(c)], the minima calculated are 18 eV ($n = 1$), 32 eV ($n = 2$), and 58 eV ($n = 3$) using the original equation, whereas the minima's positions calculated using the modified formula are 47 eV ($n = 4$), 87 eV ($n = 3$), and 86.6 eV ($n = 1$), respectively. The above results suggest that the minima of the harmonic spectrum and the results calculated using the modified two-center interference formula are in good agreement with each other. It is therefore concluded that the effect

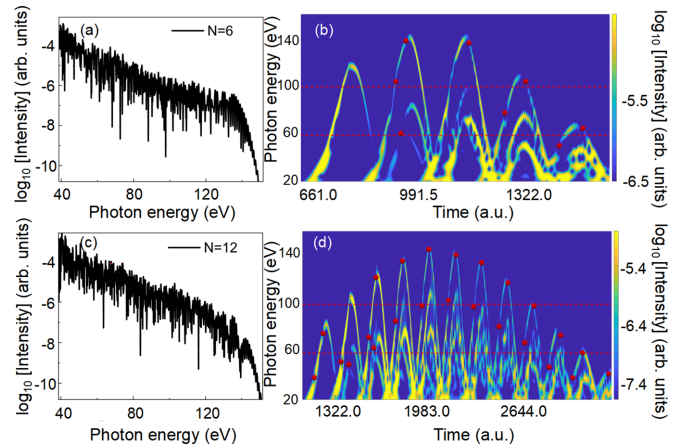


FIG. 8. (a) and (c) Harmonic spectra and (b) and (d) time-frequency analysis for $N = 6$ and $N = 12$, respectively. The red dashed lines represent the harmonic energy positions (58, 98 eV) obtained in Ref. [35]. The red circles represent the minimum positions calculated using Eq. (7).

of $\Delta\Phi(t)$ on the position of the minima can be approximately neglected in the case of small internuclear distance, whereas it cannot be neglected in the case of large internuclear distance.

Through our analysis, we clearly observe the dependence of the H_2^+ harmonic minimum position on the laser parameters. Furthermore, we study the influence of laser-pulse duration on the harmonic minimum. For $E_0 = 0.045$ and $\omega_0 = 0.019$, a laser field with a duration of six optical cycles ($N = 6$) interacts with H_2^+ at $R = 9$. The resulting harmonic spectrum [Fig. 8(a)] does not present the minimum position. However, time-frequency analysis [Fig. 8(b)] reveals multiple minima at different emission times. The calculated minimum positions from Ref. [35] at 58 and 98 eV do not fully match the observed minima in the time-frequency analysis. Using Eq. (7), the emission time can be calculated as 928.70, 948.53, 958.44, 1150.14, 1265.81, 1312.09, 1421.15, and 1490.56 a.u. The corresponding harmonic energies are 111, 58, 141, 138.3, 77.13, 101.2, 50, and 64.45 eV, respectively [shown by the red circles in Fig. 8(b)]. This result corresponds well with the positions of minima in the time-frequency analysis. When the duration of the laser field is extended to 12 optical cycles ($N = 12$), the position of the minimum in the harmonic emission spectrum is not observed [Fig. 8(c)]. However, through time-frequency analysis, the minimum position of the emission trajectory [Fig. 8(d)] can still be identified. The red dashed lines in Fig. 8(d) are the minimum positions calculated in Ref. [35] (58 and 98 eV). Therefore, neglecting the laser-field effect leads to incomplete agreement between the minimum positions calculated and the minima observed in the time-frequency analysis. However, our Eq. (7), which considers the laser-field effect, shows good agreement with the minimum positions in the time-frequency analysis. It should be noted that the time dependence of $[A(t)R]/2\pi$ in Eq. (7) leads to variations in the positions of the minima during the harmonic emission. Therefore, the contribution from different optical periods makes the minimum positions of the harmonic spectra more complicated.

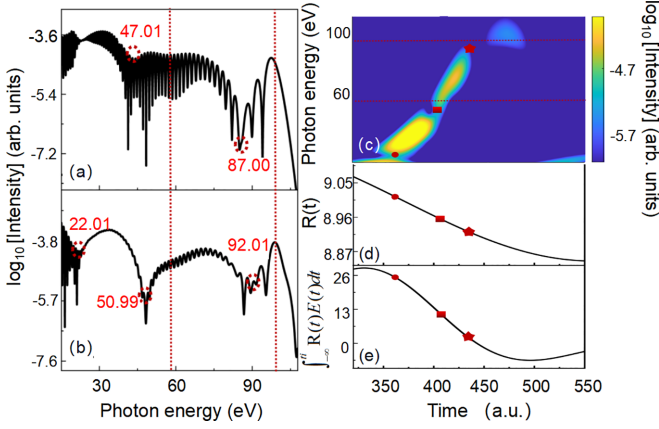


FIG. 9. (a) High-order harmonic generation (HHG) at a fixed internuclear distance for laser parameters $N = 2$, $E_0 = 0.045$, and $\omega_0 = 0.019$. (b)–(e) In the case of nuclear motions, the high harmonic spectra, the time-frequency analysis, the time-dependent internuclear distance, and the time-dependent $(A(t)R)/2\pi$, respectively.

The above analysis is carried out at a fixed internuclear distance; however, for molecular high-order harmonic generation, nuclear motion during the ionization and recombination steps plays an important role. The importance of nuclear motion in understanding the dynamics of H_2^+ driven by strong laser pulses is represented in [45,49,53–59]. We further discuss the effect of the field with a frequency of 0.019, an amplitude of 0.045, and $N = 2$ on H_2^+ with an initial internuclear distance of 9 considering the nuclear motion. The method employed is based on Eq. (3). Figure 9(a) shows the harmonic spectrum under the same laser parameters with a fixed internuclear distance. Notably, the harmonic spectrum exhibits minima near 47 and 87 eV, which differ from 58 and 98 eV [indicated by the red dashed lines in Fig. 9(a)]. According to Eq. (3), the harmonic spectrum in the case of nuclear motion is obtained, as shown in Fig. 9(b). It can be observed that the three minimum positions are 22.01, 50.99, and 92.01 eV. However, these minimum positions differ from those obtained with a fixed internuclear distance. This is because, when accounting for nuclear motion, the positions of the two nuclei themselves change, resulting in an accumulation of an additional phase. Therefore, in the case of nuclear motion, Eq. (7) is rewritten as

$$\begin{aligned} R(t_i)/\lambda + \left[\int_{-\infty}^{t_i} -R(t)E(t)dt \right] / 2\pi \\ = (n - 1/2) \quad (n = 1, 2, 3, \dots), \end{aligned} \quad (8)$$

where t_i represents the recollision time. To confirm this, we conducted a time-frequency analysis and found that the minima position at 22.01 eV [red circle in Fig. 9(c)] corresponds to a time of 362, $R(t = 362) = 9.02$ [red circle in Fig. 9(d)]. After combining the red circle position in Fig. 9(e) ($[\int_{-\infty}^{t_i} -R(t)E(t)dt]/2\pi = 22.7$), using $n = 5$, and substituting those into Eq. (8), we obtain $\lambda = 10.19$. According to $p = 2\pi\hbar/\lambda$ and $\varepsilon = p^2/2 + I_p$, the minimum position is 21.98 eV, which is consistent with the observed minimum position. When the emission time is 413 [red box in Fig. 9(c)], $[\int_{-\infty}^{t_i} -R(t)E(t)dt]/2\pi = 7.8$ [red box in Fig. 9(e)], and

$R(t = 413) = 8.95$ [red box in Fig. 9(d)], for $n = 4$, the minimum position is 50.99 eV. When the emission time is 438 [red star in Fig. 9(c)], $[\int_{-\infty}^{t_i} -R(t)E(t)dt]/2\pi = 0.99$ [red star in Fig. 9(e)], and $R(t = 438) = 8.93$ [red star in Fig. 9(d)], for $n = 4$, the minimum position is 92.01 eV. Those values correspond well with the positions of the minima. From the above analysis, it can be seen that in the case of nuclear motion, after the field action, it is necessary to include the additional accumulated phase due to the change in the distance between the two nuclei during the nuclear motion. The minimum position calculated with Eq. (8) is in good agreement with that from the harmonic spectrum. In conclusion, when nuclear motion is considered, the positions of the minima in the harmonic spectrum do not match the positions at 58 and 98 eV [indicated by the red dashed line in Fig. 9(c)] obtained without considering nuclear motion. Therefore, while the minima may change when considering the nuclear motion, accounting for the laser-field effect and internuclear distance with Eq. (8) enables accurate determination of the minimum positions.

Through the above analysis, we found that both the pulse duration and the nuclear motion affect the observation of the minimum position of the harmonic spectrum. Therefore, in order to observe the phenomenon discovered in our work, it is necessary to apply an ultrashort pulse to the alignment H_2^+ experimentally and add a prepulse to make it dissociate into a state with a large internuclear distance.

IV. CONCLUSIONS

In conclusion, we theoretically studied the harmonic minima of H_2^+ with a large internuclear distance under the action of the midinfrared driving laser. For the same intensity of laser pulse, the position of the H_2^+ harmonic minimum decreases with the increase of the driving laser frequency. At the same laser frequency, the energy of the harmonic minimum decreases with the increase of the peak amplitude of the driving laser electric field. With the analysis of the amplitude and phase of the localized states, we found that the wavelength of the harmonic minimum is determined by $R/\lambda + \Delta\Phi(t)/2\pi = (n - 1/2)$, where $n = 1, 2, 3, \dots$. In particular, the effect of $\Delta\Phi(t)$ on the position of the minimum cannot be ignored in the case of a large internuclear distance. More in-depth results showed that when nuclear motion is taken into account, the position of the minimum driven by low-intensity and ultrashort pulses satisfies $R(t_i)/\lambda + [\int_{-\infty}^{t_i} -R(t)E(t)dt]/2\pi = (n - 1/2)$, $n = 1, 2, 3, \dots$

ACKNOWLEDGMENTS

This project was supported by the National Key Research and Development Program of China (Grants No. 2019YFA0307700, No. 2022YFE0134200), the National Natural Science Foundation of China (NSFC; Grants No. 12074145, No. 11975012, and No. 12374029), and the Jilin Provincial Research Foundation for Basic Research, China (Grant No. 20220101003JC). The authors acknowledge the High-Performance Computing Center of Jilin University for supercomputer time.

- [1] A. L'Huillier, K. J. Schafer, and K. C. Kulander, *J. Phys. B* **24**, 3315 (1991).
- [2] T.-T. Fu, S.-S. Zhou, J.-G. Chen, J. Wang, F.-M. Guo, and Y.-J. Yang, *Opt. Express* **31**, 30171 (2023).
- [3] J. L. Krause, K. J. Schafer, and K. C. Kulander, *Phys. Rev. Lett.* **68**, 3535 (1992).
- [4] H. Yuan, Y. Yang, F. Guo, J. Wang, J. Chen, W. Feng, and Z. Cui, *Opt. Express* **31**, 24213 (2023).
- [5] A. D. Bandrauk, S. Chelkowski, and I. Kawata, *Phys. Rev. A* **67**, 013407 (2003).
- [6] Y. Qiao, Y. Huo, H. Liang, J. Chen, W. Liu, Y. Yang, and S. Jiang, *Phys. Rev. B* **107**, 075201 (2023).
- [7] Y. Qiao, Y.-Q. Huo, S.-C. Jiang, Y.-J. Yang, and J.-G. Chen, *Opt. Express* **30**, 9971 (2022).
- [8] A. McPherson, G. Gibson, H. Jara, U. Johann, T. S. Luk, I. McIntyre, K. Boyer, and C. K. Rhodes, *J. Opt. Soc. Am. B* **4**, 595 (1987).
- [9] Y.-J. Yang, G. Chen, J.-G. Chen, and Q.-R. Zhu, *Chin. Phys. Lett.* **21**, 652 (2004).
- [10] Y. Qiao, J. Chen, Y. Huo, H. Liang, R. Yu, J. Chen, W. Liu, S. Jiang, and Y. Yang, *Phys. Rev. A* **107**, 023523 (2023).
- [11] Y.-J. Yang, J.-G. Chen, F.-P. Chi, Q.-R. Zhu, H.-X. Zhang, and J.-Z. Sun, *Chin. Phys. Lett.* **24**, 1537 (2007).
- [12] J.-G. Chen, S.-L. Zeng, and Y.-J. Yang, *Phys. Rev. A* **82**, 043401 (2010).
- [13] F. Krausz and M. Ivanov, *Rev. Mod. Phys.* **81**, 163 (2009).
- [14] P.-C. Li, X.-X. Zhou, G.-L. Wang, and Z.-X. Zhao, *Phys. Rev. A* **80**, 053825 (2009).
- [15] C. Vozzi, M. Negro, F. Calegari, G. Sansone, M. Nisoli, S. De Silvestri, and S. Stagira, *Nat. Phys.* **7**, 822 (2011).
- [16] S. Haessler, J. Caillat, W. Boutu, C. Giovanetti-Teixeira, T. Ruchon, T. Auguste, Z. Diveki, P. Breger, A. Maquet, B. Carré, R. Taïeb, and P. Salières, *Nat. Phys.* **6**, 200 (2010).
- [17] J. Itatani, J. Levesque, D. Zeidler, H. Niikura, H. Pépin, J.-C. Kieffer, P. B. Corkum, and D. M. Villeneuve, *Nature (London)* **432**, 867 (2004).
- [18] P. B. Corkum, *Phys. Rev. Lett.* **71**, 1994 (1993).
- [19] X.-M. Tong and S.-I. Chu, *Phys. Rev. A* **61**, 021802(R) (2000).
- [20] D. Wang, X. Zhu, H. Yuan, P. Lan, and P. Lu, *Phys. Rev. A* **101**, 023406 (2020).
- [21] M. Lewenstein, P. Balcou, M. Y. Ivanov, A. L'Huillier, and P. B. Corkum, *Phys. Rev. A* **49**, 2117 (1994).
- [22] E. V. van der Zwan, C. C. Chirilă, and M. Lein, *Phys. Rev. A* **78**, 033410 (2008).
- [23] M. C. H. Wong, A.-T. Le, A. F. Alharbi, A. E. Boguslavskiy, R. R. Lucchese, J.-P. Brichta, C. D. Lin, and V. R. Bhardwaj, *Phys. Rev. Lett.* **110**, 033006 (2013).
- [24] J. B. Bertrand, H. J. Wörner, P. Hockett, D. M. Villeneuve, and P. B. Corkum, *Phys. Rev. Lett.* **109**, 143001 (2012).
- [25] J. Higuette, H. Ruf, N. Thiré, R. Cireasa, E. Constant, E. Cormier, D. Descamps, E. Mével, S. Petit, B. Pons, Y. Mairesse, and B. Fabre, *Phys. Rev. A* **83**, 053401 (2011).
- [26] O. Smirnova, Y. Mairesse, S. Patchkovskii, N. Dudovich, D. Villeneuve, P. Corkum, and M. Y. Ivanov, *Nature (London)* **460**, 972 (2009).
- [27] H. J. Wörner, J. B. Bertrand, P. Hockett, P. B. Corkum, and D. M. Villeneuve, *Phys. Rev. Lett.* **104**, 233904 (2010).
- [28] Y. Mairesse, J. Higuette, N. Dudovich, D. Shafir, B. Fabre, E. Mével, E. Constant, S. Patchkovskii, Z. Walters, M. Y. Ivanov, and O. Smirnova, *Phys. Rev. Lett.* **104**, 213601 (2010).
- [29] N. M. Gabor, Z. Zhong, K. Bosnick, J. Park, and P. L. McEuen, *Science* **325**, 1367 (2009).
- [30] T. Kanai, S. Minemoto, and H. Sakai, *Nature (London)* **435**, 470 (2005).
- [31] C. Vozzi, F. Calegari, E. Benedetti, J.-P. Caumes, G. Sansone, S. Stagira, M. Nisoli, R. Torres, E. Heesel, N. Kajumba, J. P. Marangos, C. Altucci, and R. Velotta, *Phys. Rev. Lett.* **95**, 153902 (2005).
- [32] R. Torres, T. Siegel, L. Brugnera, I. Procino, J. G. Underwood, C. Altucci, R. Velotta, E. Springate, C. Froud, I. C. E. Turcu, S. Patchkovskii, M. Y. Ivanov, O. Smirnova, and J. P. Marangos, *Phys. Rev. A* **81**, 051802(R) (2010).
- [33] M. C. H. Wong, J.-P. Brichta, and V. R. Bhardwaj, *Phys. Rev. A* **81**, 061402 (2010).
- [34] M. Lein, N. Hay, R. Velotta, J. P. Marangos, and P. L. Knight, *Phys. Rev. Lett.* **88**, 183903 (2002).
- [35] M. Lein, N. Hay, R. Velotta, J. P. Marangos, and P. L. Knight, *Phys. Rev. A* **66**, 023805 (2002).
- [36] M. Lein, P. P. Corso, J. P. Marangos, and P. L. Knight, *Phys. Rev. A* **67**, 023819 (2003).
- [37] H.-F. Cui and X.-Y. Miao, *Chem. Phys. Lett.* **731**, 136583 (2019).
- [38] Y.-C. Han and L. B. Madsen, *Phys. Rev. A* **87**, 043404 (2013).
- [39] T. Zuo and A. D. Bandrauk, *Phys. Rev. A* **52**, R2511 (1995).
- [40] A. D. Bandrauk and J. Ruel, *Phys. Rev. A* **59**, 2153 (1999).
- [41] T. Zuo, S. Chelkowski, and A. D. Bandrauk, *Phys. Rev. A* **48**, 3837 (1993).
- [42] V. Baranovski, O. Lubimova, A. Makarov, and O. Sizova, *Chem. Phys. Lett.* **361**, 196 (2002).
- [43] R. Kopold, W. Becker, and M. Kleber, *Phys. Rev. A* **58**, 4022 (1998).
- [44] R. E. F. Silva, P. Riviere, F. Morales, O. Smirnova, M. Ivanov, and F. Martin, *Sci. Rep.* **6**, 32653 (2016).
- [45] X.-B. Bian and A. D. Bandrauk, *Phys. Rev. Lett.* **113**, 193901 (2014).
- [46] K. Codling, L. J. Frasinski, and P. A. Hatherly, *J. Phys. B* **22**, L321 (1989).
- [47] M. D. Feit and J. A. Fleck, Jr., *J. Chem. Phys.* **78**, 301 (1983).
- [48] M. R. Hermann and J. A. Fleck, Jr., *Phys. Rev. A* **38**, 6000 (1988).
- [49] P. P. Corso, E. Fiordilino, and F. Persico, *J. Phys. B* **40**, 1383 (2007).
- [50] A. D. Bandrauk, S. Chelkowski, and H. Lu, *J. Phys. B* **42**, 075602 (2009).
- [51] I. Gonoskov, M. Y. Ryabikin, and A. Sergeev, *J. Phys. B* **39**, S445 (2006).
- [52] H. Wind, *J. Chem. Phys.* **42**, 2371 (1965).
- [53] L. Yue and L. B. Madsen, *Phys. Rev. A* **93**, 031401(R) (2016).
- [54] R. E. F. Silva, F. Catoire, P. Rivière, T. Niederhausen, H. Bachau, and F. Martín, *Phys. Rev. A* **92**, 013426 (2015).
- [55] R. E. F. Silva, F. Catoire, P. Rivière, H. Bachau, and F. Martín, *Phys. Rev. Lett.* **110**, 113001 (2013).
- [56] C. B. Madsen, F. Anis, L. B. Madsen, and B. D. Esry, *Phys. Rev. Lett.* **109**, 163003 (2012).
- [57] F. Catoire, R. E. F. Silva, P. Rivière, H. Bachau, and F. Martín, *Phys. Rev. A* **89**, 023415 (2014).
- [58] F. Morales, P. Riviere, M. Richter, A. Gubaydullin, M. Ivanov, O. Smirnova, and F. Martin, *J. Phys. B* **47**, 204015 (2014).
- [59] M. Lara-Astiaso, R. E. F. Silva, A. Gubaydullin, P. Rivière, C. Meier, and F. Martín, *Phys. Rev. Lett.* **117**, 093003 (2016).